Chinese Chemical Letters 31 (2020) 2634–2640

Contents lists available at ScienceDirect

Chinese Chemical Letters

journal homepage: www.elsevier.com/locate/cclet

Communication

An old story with new insight into the structural transformation and radical production of micron-scale zero-valent iron on successive reactivities

Xinhao Wang[a,b], Xueting Pu[a,b], Yue Yuan[c], Yunjie Xiang[a,b], Yuling Zhang[a,b], Zhaokun Xiong[a,b,*], Gang Yao[b,d], Bo Lai[a,b,*]

[a] State Key Laboratory of Hydraulics and Mountain River Engineering, College of Architecture and Environment, Sichuan University, Chengdu 610065, China
[b] Sino-German Centre for Water and Health Research, Sichuan University, Chengdu 610065, China
[c] National Engineering Laboratory for Clean Technology of Leather Manufacture, College of Biomass Science and Engineering, Sichuan University, Chengdu 610065, China
[d] Institute of Environmental Engineering, RWTH Aachen University, Aachen 52062, Germany

ARTICLE INFO

Article history:
Received 30 June 2020
Received in revised form 15 July 2020
Accepted 5 August 2020
Available online 23 August 2020

Keywords:
Zero-valent iron
Iron oxides
p-Nitrophenol
Structural transformation
Successive reactivities

ABSTRACT

It is generally recognized that the formation and accumulation of iron oxides on the surface of zero-valent iron (Fe^0) resulting in significant decrease of contaminant degradation rates during the long-term reactions. However, in this study, we found that the removal efficiencies of *p*-nitrophenol (PNP) by micro zero-valent iron (mFe^0) could maintain at the satisfactory level in the process of continuous reactions (20 cycles). The removal rate constant (0.1779 min^{-1}) of the 5th cycle was 6.74 times higher than that of the 1st reaction (0.0264 min^{-1}), even the 20th cycle (0.0371 min^{-1}) was higher than that of the 1st reaction. Interestingly, almost no dissolved iron was detected in the solution, and the total iron concentrations decreased dramatically with the process of continuous reactions. The results of scanning electron microscope and energy dispersive spectrometry (SEM-EDS) and X-ray diffraction (XRD) revealed that the structure and composition of corrosion products change from amorphous to highly crystal with the increase of the number of cycles. The corrosion products were mainly magnetite (Fe_3O_4) and a small part of maghemite (γ-Fe_2O_3), which were in the form of microspheres on the surface of mFe^0. The formation of surface oxidation shell hindered the release of Fe^{2+}. X-ray photoelectron spectroscopy (XPS) results illustrated that partial Fe_3O_4 could be converted into γ-Fe_2O_3. Electrochemical analysis proved that the electron transfer rate of mFe^0 increased with the formation of the oxides shell. However, the consumption of iron core and thicker oxide film weakened the electron transfer rate. Besides, the quenching experiments indicated that the reaction activity of mFe^0 could be enhanced with the addition of scavengers. This study deepened the understanding of the structural transformation and radical production of mFe^0 in continuous reactions.

In the past few decades, zero-valent iron (Fe^0) has been wildly employed for various contaminants removal including halogenated organics, nitro-aromatics, heavy metals, and oxy-anions due to the advantages of low cost, environment-friendly and low redox potential (E^0 = –0.44 eV) [1]. As we all know, there are various iron corrosion products formed during the corrosion of Fe^0, which can degrade the contaminants *via* adsorption, reduction, and co-precipitation [2–4]. Up to now, despite the extensive research on Fe^0, the traditional Fe^0 still suffering from several challenges including its essential passive layer, narrow working pH, and reactivity loss after long-term operation due to the reaction of Fe^0 with water and oxygen to form iron (hydr)oxides [3,5]. However, our previous work found that the degradation efficiencies of pollutants by micron-scale Fe^0 (mFe^0) were elevated with the successive treatment [6]. This phenomenon was diverse from the previous consequence in the aging process of Fe^0.

It's reported that the Fe^0 particles will form an oxide film in the air, which is mainly composed of the inner shell (magnetite) and the outer shell (hematite) [7–9]. Electrons can transfer freely in the magnetite layer, but the outer layer of hematite has a great

* Corresponding authors at: State Key Laboratory of Hydraulics and Mountain River Engineering, College of Architecture and Environment, Sichuan University, Chengdu, 610065, China.
E-mail addresses: scuxzk@scu.edu.cn (Z. Xiong), laibo@scu.edu.cn (B. Lai).

https://doi.org/10.1016/j.cclet.2020.08.007
1001-8417/

hindrance to the transmission of electrons [10]. Besides, long-term batch studies have believed that the primary or secondary mineral precipitation such as magnetite (Fe_3O_4), lepidocrocite (γ-FeOOH) and green rust can sustain the Fe^0 reactivity, but the hematite (α-Fe_2O_3), goethite (α-FeOOH) and magnetite (γ-Fe_2O_3)) can decrease the performance of Fe◦ for contaminants removal [11–13]. The various corrosion products have opposite effects on the activity of Fe^0. Besides, some researchers found that the reaction of Fe^0 with O_2 can produce reactive oxygen species (ROS) to oxidize both inorganic and organic compounds [14,15]. Thus, besides structural transformation of Fe^0, the free radicals produced in the presence of oxygen will certainly make some contribution in long-term reaction. As mentioned above, numerous investigations on the oxidation/passivation and free radicals of the Fe^0 system were reported. However, there are rare studies on the influence of structural revolution and free radical transformation of Fe^0 in successive reactions on the pollutant removal process, and the relative mechanism is not always clear.

Therefore, the primary objective of this work is focus on the changes of reactivity, structure and free radicals of mFe^0 in continuous operation process. Presently, most of the researches were concerning the nanoscale zero-valent iron (nFe^0). However, we have limited insight into the short or medium-term corrosion processes on mFe^0 surface nor do we know the key parameters in cyclic experiments. We choose *p*-nitrophenol (PNP) as the model pollutant because of its highly toxic, carcinogenic, bioaccumulation and easily detected intermediates [16–18]. The purposes of this study are to (i) explore the degradation of PNP by mFe^0 in the cyclic process, (ii) reveal the morphological, structural, and compositional evolution of mFe^0 during the continuous reactions, (iii) clarify the influence concerning to PNP removal by free radicals in mFe^0 system.

To investigate thoroughly the reactivity and recyclability of mFe^0 in the consecutive process, the experiment was conducted for 20 cycles (the detailed information of materials and methods is provided in Supporting information). As shown in Fig. 1a, the removal rate of PNP in the whole process can be divided into three periods: (i) The removal rates increased with the cycle (from the 1st cycle to the 5th cycle), (ii) the removal rate gradually and persistently increased and then reached a relative plateau (from the 6th cycle to the 12th cycle), (iii) the ability of reduction decreased with the aging time (from the 13th cycle to the 20th cycle). In the period (i), the removal rate of PNP almost displays a gradient increase. In the next stage, the removal rate of PNP maintained at 100.0% after 30 min. However, the removal rate of PNP gradually decreased from 100.0% to 69.0% in the period of (iii). Additionally, to give a clear comparison of the removal performance, the PNP removal kinetics were fitted by the *pseudo*-first-order kinetic reaction (Fig. S1 in Supporting information). The kinetic analysis indicates that the degradation efficiencies of PNP with different cycles all were described by the *pseudo*-first-order and the correlation of determinations (R^2) were all greater than 0.95, as shown in Fig. S1 (Supporting information). It was observed that the k_{obs} for PNP removal of the 5th cycle (0.1779 min^{-1}) was 6.74-fold greater than the first time (0.0264 min^{-1}) in Figs. S1a and S2 (Supporting information). This result was mainly attributed that the pre-existing oxidation film of mFe^0 was destructed in the process of contact with water. The core of mFe^0 was exposed and more active sites were exposed, which enhanced the corrosion effect of mFe^0 core and promoted the degradation rates of PNP swiftly [10,19,20].

Besides, it can be found in Fig. S3 (Supporting information) that the amount of precipitate in the effluent (the mFe^0 particles were fixed at the bottom of the reactor by a magnet and then take out the effluent sample from the homogeneous phase) decreased gradually with the process of continuous reactions. Interestingly, there was almost no precipitate in the effluent after the 5th cycle. Furthermore, as shown in Fig. 1b, the concentration of dissolved iron rapidly increased to the highest level for 5 min, but there were little dissolved iron left in the solution after 30 min of treatment in the initial three cycle reactions. As usual, the concentration of total iron was at a high level (Fig. S4 in Supporting information). This phenomenon was perhaps attributed to that the released Fe^{2+} was rapidly oxidized to Fe^{3+} and formed iron oxides (hydroxides) following Eqs. 1 and 2. Meanwhile, the rapid increase of pH (Fig. S5 in Supporting information) suppressed the release of iron ions, but the iron oxides and hydroxides continued to grow [21]. Surprisingly, after the former reactions, the concentration of dissolved iron couldn't be detected, and even the total iron concentration of the solution was plummeted (from 73.81 mg/L to 18.85 mg/L), as shown in Figs. 1b and S4. Subsequently, both of the dissolved iron concentrations and the total iron concentration remained at a low level. It can be seen that there is a relationship between the transformation of iron ion and the removal of PNP. In the period (i), a large number of iron ions were released into the solution in the first 5 min due to the rapid corrosion of the iron core under acidic condition. Then, the released Fe^{2+} was oxidized to oxides dispersed in the solution or deposited on the surface of iron to form an oxidation film. Dissolved iron was almost not detected in the period (ii), the total iron was much lower than that in the period (i), and the removal rate of PNP reached a peak and remained stable. On the one hand, the formation of oxide film not only increase the absorption capacity of mFe^0, but also accelerates the electronic transfer from the core to the surface, so the reduction of pollutants is greatly improved [10]. On the other hand, these fluctuations in reactivity connected with the rapid destruction of the original Fe^{3+} oxide film on mFe^0 in the process of PNP treatment, and the subsequent formation of a new passivating mixed-valence Fe^{2+}-Fe^{3+} oxide shell [10,22,23]. Also, there was a rapid destruction of outer film during each washing process, which can enhance the

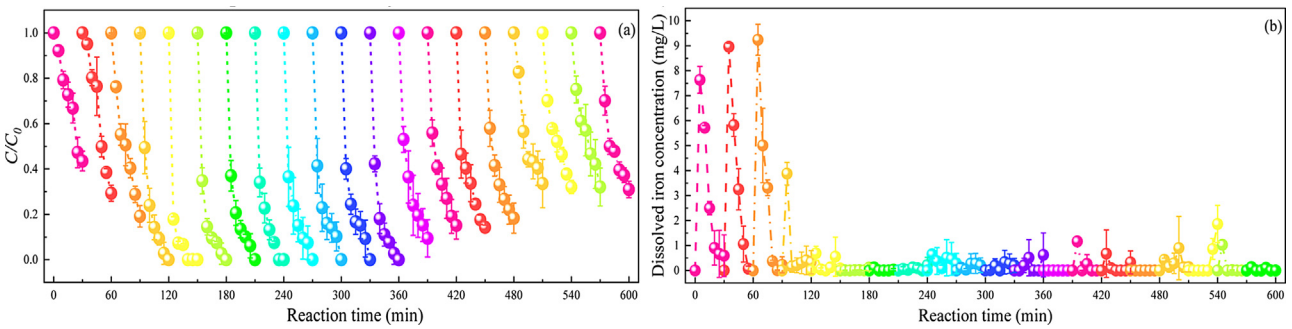

Fig. 1. Comparison of performance for 20 successive treatments on (a) the removal rates of PNP and (b) the concentration of dissolved iron ions (reaction condition: $[PNP]_0 = 100$ mg/L, $[mFe^0]_0 = 10$ g/L, $[Na_2SO_4]_0 = 10$ mmol/L, initial pH 5.6).

reactivity of mFe^0 in the following cycles. Hence, we assumed that the structure of mFe^0 changes with the cycle reaction process, which played a significant role in the mass transfer tempo of the pollutants, intermediates, and corrosion products between the mFe^0 and the liquid phase. When the disruptions of the pre-existing oxide film, the corrosion of the iron core were strengthened. Simultaneously, with the release of Fe^{2+} and the consumption of H^+, the solution pH would increase. As shown in Fig. S5, the solution pH during mFe^0 reaction exceeded 7.0 from initial pH of 5.6 and then reached 9.6 maximally in the whole 20 cycle reaction processes, which were following the previous results of Fe^0 catalysts [24,25]. Furthermore, the reason why the pH of the solution was declined is that the Fe^{3+} was hydrolysis following Eq. (3) and the oxidation rate of Fe^{2+} is higher than the corrosion rate of Fe^0. Notably, when solution pH increased to the range of 7.0–8.0, the mFe^0 corrosion would alter their pathway to Eq. (4) where no proton consumption or generation took place, so as the pH kept almost constant [26,27]. This explained why there were a lot of reddish-brown flocculent precipitates in the initial three cycle reactions of effluent, as shown in Fig. S3.

$$2Fe^0 + O_2 + 2H_2O \rightarrow 2Fe^{2+} + 4OH^- \quad (1)$$

$$4Fe^{2+} + O_2 + 2H_2O \rightarrow 4Fe^{3+} + 4OH^- \quad (2)$$

$$Fe^{3+} + 3H_2O \rightarrow Fe(OH)_3 + 3H^+ \quad (3)$$

$$4Fe^0 + 3O_2 + 6H_2O \rightarrow 4Fe(OH)_3 \quad (4)$$

The aforementioned results reveal that the reactivity of mFe^0 could be profoundly improved. We speculate that the change of mFe^0 surface structure and radicals are responsible for the enhancement of the PNP removal rate. Therefore, additional experiments should be performed to investigate the effects of details of surface structure and radicals.

Scanning electron microscope (SEM) and energy dispersive spectrometry (EDS) were utilized to characterize the change of morphology and the weight ratio of elements on the surface of aged mFe^0 particles including 1st, 2nd, 3rd, 4th, 5th, 6th, 12th, 13th, 17th, 20th cycles, which had a strong transformation of the removal rate of PNP. The SEM images were shown in Figs. 2 and S6 (Supporting information), the shape of mFe^0 surface appeared different from each other in the whole aging process. For fresh mFe^0, the surface was smooth and dense [28,29]. The surface of the mFe^0 particle was smooth at low magnification after 30 min of reaction (Fig. 2A), while some flaky substances can be observed on the surface of mFe^0 at high magnification (Fig. 2a). Then, with the increase of cycles, it can be observed that the amount of submicron scale spherical corrosion products (most of the corrosion products were smaller than 1 μm) were formed on the surface of mFe^0, and the flaky corrosion products were almost invisible (Figs. 2b–j). It also confirms that the accumulation of oxides on the surface gradually increases and the core-shell structure is formed. Besides, it can be found that the globular materials covered on the surface of mFe^0, the reaction rate increased significantly, which implied that this oxide layer can promote the removal efficiency of PNP. However, this promotion effect does not last as the growth of surface products. When it reached a certain degree, as shown in Figs. 2G–J, its reactivity declined with the increase of surface deposit. The results indicated that a medium thickness of the shell has a high-level conductivity, but the over-thick oxide shell weakened the reduction capacity. It can be seen from the SEM-EDS results (Fig. S7 and Table S1 in Supporting information) that the

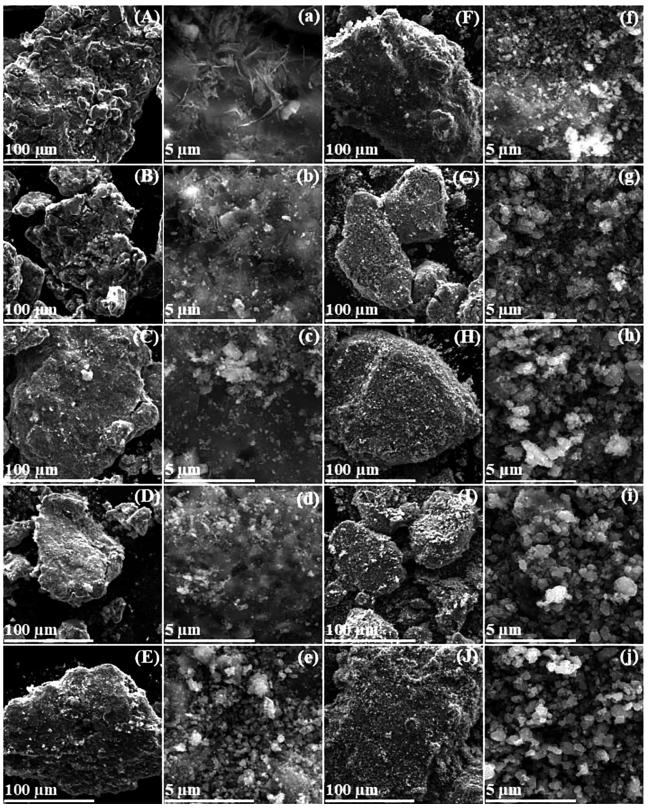

Fig. 2. The representative SEM images of mFe^0 particles after various cycle reactions at different magnification: (A) and (a) correspond to the mFe^0 after the first reaction, and each group is the same correspondence rule (A, a-1st; B, b-2nd; C, c-3rd; D, d-4th; E, e-5th; F, f-6th; G, g-12th; H, h-13th; I, i-17th; J, j-20th).

weight ratio of Fe and O in mFe^0 was 15.26% and 84.74% respectively at the end of the first reaction. It indicated that the surface of mFe^0 was oxidized in the PNP at initial pH 5.6. Table S1 shows that the mass fraction proportion of oxygen was increasing, which indicated that the iron oxides accumulated gradually in the successive cycle processes.

To further confirm the ingredient of these corrosion products, the mFe^0 particles were further analyzed by X-ray diffraction (XRD) based on SEM-EDS analysis. The peaks at 45° and 65° should be assigned to Fe^0 [30]. Fig. 3 revealed that the XRD patterns of 1st aged mFe^0 particles (after the 1st reaction) were consistent with the fresh one and there is no new characteristic peak. However, the result of SEM-EDS shows that amorphous and/or crystalline iron

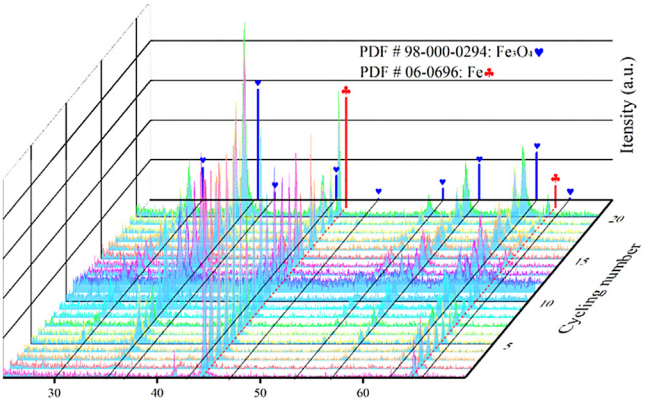

Fig. 3. XRD analysis of mFe^0 reacted with PNP in successive reaction for 20 cycles.

(hydro)oxides generate on the mFe^0 surface. Hence, the corrosion products were maybe amorphous iron (hydr) oxides [6]. Besides, XRD analysis reveals that characteristic peaks matched with magnetite (Fe_3O_4) became more distinct and stronger with the progress of cycle time. When mixed with water, the mFe^0 reacted with H_2O/O_2 to form hydroxides or oxyhydroxides as shown in Eqs. 5–7 [31].

$$6Fe^{2+} + O_2 + 6H_2O \rightarrow 2Fe_3O_4(s) + 12H^+ \quad (5)$$

$$Fe^{2+} + 2OH^- \rightarrow Fe(OH)_2(s) \quad (6)$$

$$6Fe(OH)_2(s) + O_2 \rightarrow 2Fe_3O_4 + 6H_2O \quad (7)$$

As we can see from Fig. 3, the intensity of mFe^0 peaks gradually weakens, and the peaks of Fe_3O_4 start to emerge and strengthen. The results indicated that the formation of Fe_3O_4 in a certain period (from the 1st cycle to 12th cycle) does enhance the removal rate of PNP. The formation of magnetic layer forms a thin and stable semiconductor film under a certain thickness, which enhances the ability of the internal iron to release electrons to the outside, thereby directly reducing pollutants [10,32]. Besides, the transformation of poorly crystalline iron oxides to highly crystalline iron oxides due to the electron transfer between Fe^{2+} and Fe^{3+} and the corrosion of internal iron core [33]. Dong *et al.* also reported that after 60 days of aging, the magnetite and/or maghemite were the dominant corrosion products for the bare nFe^0 [30]. On the one hand, it's reported that the inverted spinel structure was the main existing form of Fe_3O_4, in which Fe^{2+} and the half of Fe^{3+} were in an octahedral oxygen environment, while another half of Fe^{3+} existed in a tetrahedral oxygen environment [31,34]. In the presence of oxygen, the Fe^{2+} present in Fe_3O_4 was oxidized to Fe^{3+}, resulting in the formation of γ-Fe_2O_3, without a change in the crystal structure [31]. Hence, the decrease in the reactivity of mFe^0 after the 12th cycle can be attributed to the Fe_3O_4 semiconductor layer on the surface of mFe^0 gradually transformed to γ-Fe_2O_3 passivation layer, which hindered the electron transfer from the iron core [13]. However, the characteristic peaks of γ-Fe_2O_3 cannot be found in XRD might due to the peaks of γ-Fe_2O_3 and Fe_3O_4 are very close in XRD patterns [35]. On the other hand, the decrease of PNP reduction efficiency attributed to the degree of corrosion, which means that the layer of Fe_3O_4 is too thick to transport electrons from mFe^0 to PNP. To confirm the interactions between mFe^0 core and Fe_3O_4 shell, pure Fe_3O_4 particles were used to compare with the mFe^0 after the 20th cycle for PNP removal. As shown in Fig. S8 (Supporting information), k_{obs} of mFe^0 after the 20th cycle was 4.12 times than that of Fe_3O_4. Hence, the consequence of the interactions between mFe^0 and Fe_3O_4 coatings is sensible.

To further identify the composition and chemical state of aged mFe^0, X-ray photoelectron spectroscopy (XPS) was employed to characterize the aged mFe^0 particles. The survey scan (Fig. S9 in Supporting information) showed the presence of Fe 2p, O 1s, and C 1s. The C 1s signal at 284.8 eV is used to correct the binding energy so that the acquired spectra are calibrated. High resolution of Fe 2p spectra were used to analyze the different valence states of iron (Fig. S10 in Supporting information). The results illustrated that four peaks could be observed in fresh mFe^0 particles, the peak at 710.5 and 723.8 eV correspond to Fe^{2+} species, the peaks located at 712.6 and 726.1 eV are characteristic of Fe^{3+}, and the peak at 706.2 eV proves the presence of Fe^0, which indicates that an oxide film formed on the surface of fresh mFe^0 [5,36,37]. Moreover, the position of the peaks at 718.9 eV and 732.9 eV are satellite peaks for Fe^{3+}. The similar peak positions corresponding to Fe^{3+} and Fe^{2+} were found in Fe 2p spectra of the aged mFe^0 samples (Fig. 4), which testifying that the surface of mFe^0 was covered with oxides

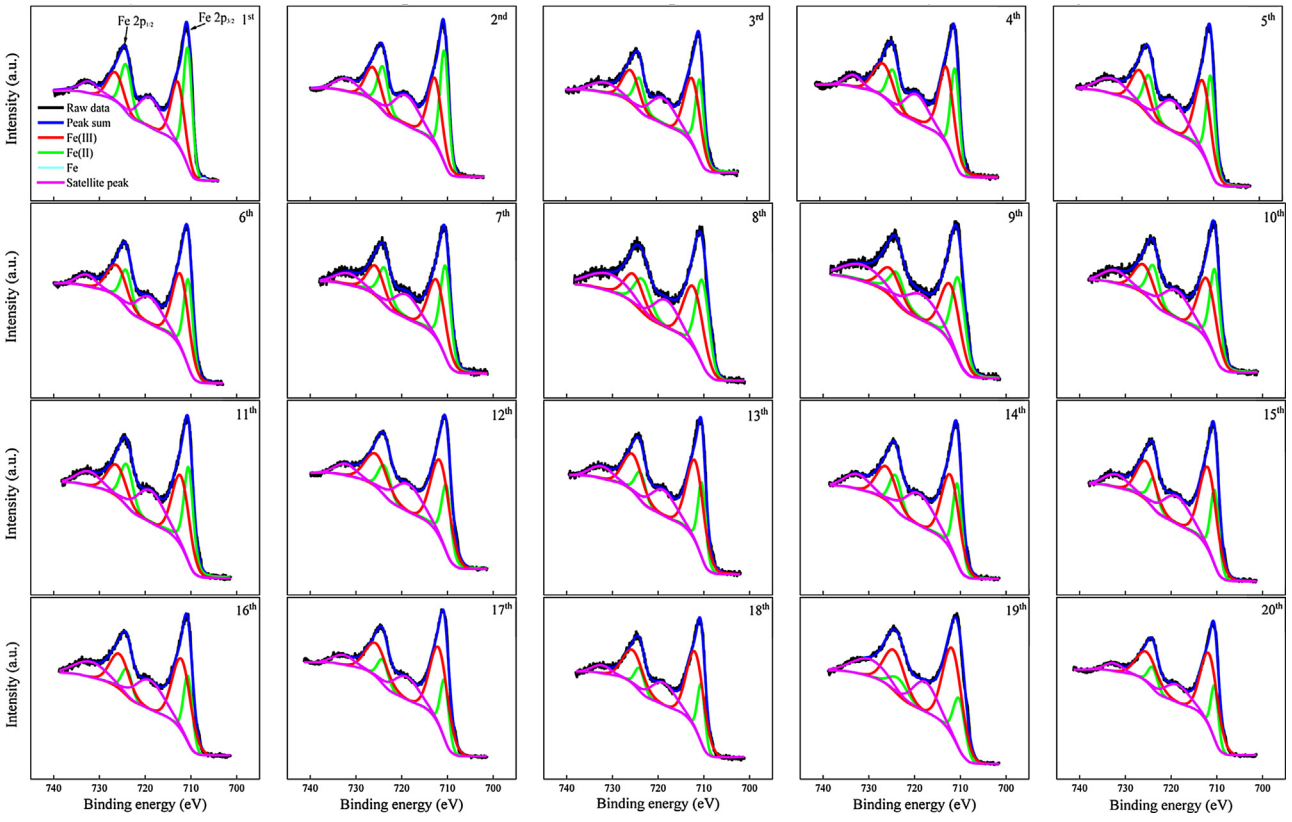

Fig. 4. 1st–20th are the XPS spectra of Fe 2p core level for aging mFe^0.

film [5,38,39]. However, the peak of Fe^0 almost disappeared in the following XPS analyses. A reasonable explanation is the sampling depth of XPS for metal oxide is less than 10 nm [5,40]. In addition, to further identify the transformation of iron oxides in cycling processes, the molar ratios of the ferrous iron to the total iron (Fe^{2+}/Fe_{total}) and ferric iron to the total iron (Fe^{3+}/Fe_{total}) were calculated by the fitting peak areas of Fe 2p core level spectra, respectively. Table S2 (Supporting information) showed a general trend that the fraction of Fe^{3+} increased progressively while that of Fe^{2+} declined with the process of continuous reactions. It proves that the bond Fe^{2+} participated in the reduction of PNP. Interestingly, the molar ratios of Fe^{2+}/Fe_{total} for the 4th (0.3012), 5th (0.3110), and 6th (0.3153) are close to the theoretical value of Fe_3O_4 (0.3333) [37]. The molar ratio of Fe^{2+}/Fe_{total} maintained a relative plateau (0.3441–0.3531) from the 7th to the 11th cycle, and then gradually decreased to 0.1705 at the end of 20th cycle. The results further suggest that when the surface composition is closed to Fe_3O_4, it has the most significant effect on PNP removal. In addition, the ratios for Fe^{2+}/Fe_{total} was fluctuation, suggesting that fresh Fe^{2+} continuously be produced during the cycle (Table S2). Therefore, it is considered that there is a cycle of Fe^{2+} and Fe^{3+} on the surface of mFe^0 [41]. At the same time, the surface Fe^{2+} was gradually oxidized to Fe^{3+} by dissolved oxygen (Eq. 8) [31,42]. The proportion of Fe^{3+} also began to increase from the 12th cycle, which indirectly confirmed that γ-Fe_2O_3 was generated. Besides, it is reported that 718.9 eV satellite peaks prove the existence of γ-Fe_2O_3 [39].

$$6Fe_3O_4 + O_2 + 4H^+ \rightarrow 8\gamma\text{-}Fe_2O_3 + 2Fe^{2+} + 2H_2O \quad (8)$$

Besides, High resolution of O 1s spectra can be divided into three peaks (Figs. S11and S12 in Supporting information). The peak at 530.0 eV is assigned to the lattice oxygen (O_2^-), which confirmed the existence of Fe_3O_4 and/or γ-Fe_2O_3 [6,43]. Another peak at 531.6 eV was interpreted as oxygen in a single bond of the hydroxyl group adsorbed at the surface of mFe^0 [43]. And the peak at 533.6 eV belongs to the chemically or physically adsorbed water [5,44–46]. Table S3 (Supporting information) illustrated that the ratio of O_2^-/O_{total} increased with the cycling numbers. The results indicate that the main corrosion products were Fe_3O_4 and/or γ-Fe_2O_3. Concurrently, the increase of O_2^- also proved that the oxidation products were continually accumulating.

As result verified above, the formation of more crystalline magnetite in partially oxidized mFe^0 upon aerobic condition. The previous study reported that the oxide film mediates electron transfer from Fe^0 to the contaminant by acting as a semiconductor [5]. The electron transfer is bound up with the oxidation of iron core, being reflected by its free corrosion potential. The more negative free corrosion potential value corresponds to a higher electron transfer rate [47–49]. To further clarify the promoting effect of oxide shell on electron transfer, we investigated the electron transfer activity of aged mFe^0 particles by measuring their free corrosion potential with Tafel polarization diagrams. The Tafel plots show that the free corrosion potential of aged mFe^0 (after 1st reaction) was –0.72 V, indicating that the electron transfer ratio was enhanced compared with the fresh one (–0.44 V), as shown in Fig. S13 (Supporting information). We continuously measured the corrosion potential of following aged mFe^0 particles including 1st, 2nd, 3rd, 4th, 5th, 6th, 12th, 13th, 17th and 20th. With the increase of cycling rounds and the accumulation of Fe_3O_4 on the surface of mFe^0, the absolute value of free corrosion potentials increases gradually (2nd: –0.78 V, 3rd: –0.79 V, 4th: –0.81 V and 5th: –0.83 V) in the period (i). During the period (ii), the potential shifted from –0.82 V to –0.80 V, suggesting that the appropriate thickness of the oxide shell can maintain the electron transfer rate at a high level. It indicated that a large number of electrons released from the iron core, which can directly reduce PNP and maintain the cycle of Fe^{2+} and Fe^{3+} on the surface of mFe^0 through the thin and stable oxidation shell. As we assumed that the electron transfer ratio began to decrease in the period (iii). The reason is that the transformation of γ-Fe_2O_3 hindered the electronic transmission ability. Nevertheless, the free corrosion potential of aging mFe^0 was still more negative than –0.44 V after 20 cycles. Hence, it is rational to conclude that the formation of Fe_3O_4 on the mFe^0 surface to form a core-shell structure can enhance the electron transfer efficiency to reduce the PNP, but the overwrapped oxide shell and the transformation of γ-Fe_2O_3 can decline the ability of aged mFe^0.

To reveal the possible existent effect of ROS on PNP removal by mFe^0 under the aerobic conditions, we conducted a series of quenching experiments with the addition of scavengers. The *tert*-butyl alcohol (TBA) and isopropanol (IPA) were carried out to detect the existence of hydroxyl radical ($^{\bullet}OH$) [25,50]. The results were shown in Fig. S14 (Supporting information), which shows different trends as we previously divided the whole process into three periods. In the period (i) and (ii), the PNP removal rates were slightly depressed in the presence of IPA and TBA, which revealed the little contribution of $^{\bullet}OH$ in mFe^0 system. However, it is observed in the period (iii) that the addition of TBA and IPA could enhance the removal efficiency of PNP by nearly 10%–15%. It is reported that $^{\bullet}OH$ yield is closely related to Fe^{2+} species [51]. To make sure that the reaction system produced $^{\bullet}OH$ and how $^{\bullet}OH$ to changed, $^{\bullet}OH$ production and surface oxidation degree of Sca-mFe^0 (the mFe^0 particles were taken after the quenching experiments with addition of scavengers) were employed to further evaluate the reason for the enhancement of PNP removal efficiency. As shown in Fig. S15 (Supporting information), the accumulated $^{\bullet}OH$ is over 29.8 μmol/L at 5 min for all 20 rounds. The trend of $^{\bullet}OH$ accumulation is consistent with the variation of solution pH (Fig. S5). Because the original solution was acidic and contained hydrogen ions (H^+), some H^+ were adsorbed on the surface of mFe^0 to form atomic hydrogen ($H^{\bullet}$) following Eq. 9, but the generated $H^{\bullet}$ could be quickly scavenged by dissolved O_2 to produce $HO_2^{\bullet}$ and H_2O_2 (Eqs. 10–12), which then would convert to $^{\bullet}OH$ [25].

$$Fe^0 + 2H^+ \rightarrow 2H^{\bullet} + Fe^{2+} \quad (9)$$

$$H^{\bullet} + O_2 \rightarrow HO_2^{\bullet} \quad (10)$$

$$HO_2^{\bullet} + H^{\bullet} \rightarrow H_2O_2 \quad (11)$$

$$H_2O_2 + Fe^{2+} \rightarrow Fe^{3+} + {}^{\bullet}OH + OH^- \quad (12)$$

$$Fe^{3+} + H_2O_2 \rightarrow HO_2^{\bullet} + H^+ + Fe^{2+} \quad (13)$$

$$2Fe^{3+} + Fe^0 \rightarrow 3Fe^{2+} \quad (14)$$

Besides, the XRD patterns (Fig. S16 in Supporting information) show that the aged Sca-mFe^0 particles have the typical diffraction peaks for magnetite and Fe^0. To further justify the influence of the addition of scavengers to the surface structure of Sca-mFe^0, Sca-mFe^0 particles after 13th, 17th, and 20th cycle were further determined by XPS analysis. The surface Fe^{2+}/Fe_{total} of Sca-mFe^0 increased from 0.2759, 0.1891 and 0.1705 to 0.3759, 0.3584, and 0.3537 compared to the mFe^0 after the 13th, 17th, and 20th reactions, respectively (Fig. S17 in Supporting information, Tables S2 and S4). XPS spectra of O 1s also indicate a slight decrease of surface O_2^-

compared to that without the addition of TBA and IPA, as shown in Fig. S17 and Table S5 (Supporting information).

Collectively, the reduction effect of mFe^0 to PNP is enhanced with the addition of TBA and IPA. The rapid quenching of $^{\bullet}OH$ shifted the Eq. 12 to the positive direction. Thus, the generation of Fe^{2+} would be promoted by the Eqs. 13, 14 [50]. From the analysis of XRD and XPS, it is considered that the generation rate Fe^{2+} is higher than that of Fe^{3+} in the Sca-mFe^0 system. At the same time, it is reported that the surface bond Fe^{2+} has a strong reduction ability and can effectively remove the adsorbed contaminants. XPS results also happen to show that the amount of Fe^{2+} bonded on the surface is also increased compared with the components without scavengers. Thus, it is reasonable that the addition of TBA and IPA slowed down the accumulation of iron oxide (*e.g.*, γ-Fe_2O_3) on the outer surface, which kept the oxidation shell in a state of high electron transport capacity. In addition, $^{\bullet}OH$ is indeed produced in the whole process of PNP removal by mFe^0, but it did not play a leading role in the removal of PNP. Generally, because the reaction is exposed to the air, active oxides are produced, which have a small negative feedback effect on the reduction reaction. The addition of TBA and IPA suppresses these active oxides and enhances the reduction of PNP.

According to the above results and analysis, the reduction of PNP is a dynamic process by mFe^0, under the condition of continuous cycle reaction. Scheme 1 thoroughly illustrates the dynamic reaction mechanisms of the cyclic process. The results for the aforementioned are summarized as four aspects. Firstly, the formation of iron (hydrogen) oxides can increase the specific surface area of these particles, thus improving the connection between particles and solutions [28]. Secondly, the oxide film transfers electrons from mFe^0 to pollutants in the form of the semiconductor. However, there is a certain relationship between the electron transfer efficiency and the stacking degree of the oxide film. In the short run, the main corrosion production of mFe^0 is Fe_3O_4. When the accumulation of Fe_3O_4 reaches an intermediate value (relative to the aging process of 20 cycles), suggesting that a thin and stable core-shell structure is formed, the ability of electron transfer could be greatly enhanced, and the cycle of the Fe^{2+} and Fe^{3+} is improved. Otherwise, the excessive accumulation of Fe_3O_4 forms a thicker oxide shell and partial Fe_3O_4 transforms to γ-Fe_2O_3, which weakens the electron transfer efficiency. Furthermore, the formation of the outer shell can prevent dissolved Fe^{2+} to release from the iron core to the solution. The scavenger experiments show that the Fe^{2+} increase compared with the experiments without scavengers, and the removal efficiency of PNP is improved. Finally, the presence of $^{\bullet}OH$ might be not conducive to PNP reduction. The presence of scavengers can restrain the detrimental effect of $^{\bullet}OH$, and then accelerate the removal rate of PNP by aged mFe^0.

In this study, we explored the dynamic changes of the reaction activity of mFe^0 in the cyclic reaction process. Several complementary characterization methods expounded the effects of structural transformation and radical production on the removal of PNP. We found that the structure and composition of mFe^0 change with the cyclic numbers when exposed to water. The continuous reactions led to the formation of mainly Fe_3O_4 and a little γ-Fe_2O_3. These oxides were uniformly distributed on the surface of mFe^0 in the form of microspheres to form a core-shell structure, which enhanced the electron transfer rate from the iron core to the outside due to the mediation of the oxidation film. However, the alleviation of the molar ratios of Fe^{2+}/Fe_{total} would decline the removal rate of PNP. Besides, one of the most probable accountabilities for the influence of radical is the consumption of surface reactive Fe^{2+} species. While the surface Fe^{2+}/Fe_{total} of Sca-mFe^0 could be recovered in the presence of scavengers, which enhanced the reduction of PNP. Therefore, the reactivity of aged mFe^0 is a dynamic process with the increasing of reaction cycles. If this process can be regulated reasonably, mFe^0 will be more prominent in wastewater treatment.

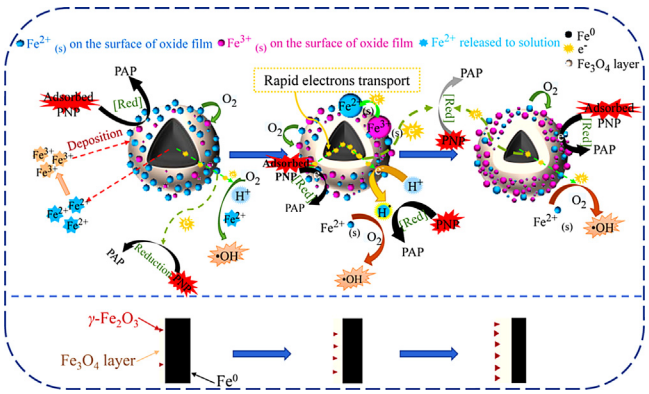

Scheme 1. The dynamic reaction mechanisms of mFe^0 for PNP removal during cyclic processes.

Declaration of competing interest

The authors report no declarations of interest.

Acknowledgments

The authors would like to acknowledge the financial support from China Postdoctoral Science Foundation (No. 2019T120843), and Sichuan Science and Technology Program (No. 2019YJ0091).

Appendix A. Supplementary data

Supplementary material related to this article can be found, in the online version, at doi:https://doi.org/10.1016/j.cclet.2020.08.007.

References

[1] J. Xu, Y. Wang, C. Weng, et al., Environ. Sci. Technol. 53 (2019) 5936–5945.
[2] Z. Yang, X. Ma, C. Shan, Z. Fang, B. Pan, Chemosphere 197 (2018) 494–501.
[3] C. Noubactep, Water Res. 85 (2015) 114–123.
[4] S. Bae, R.N. Collins, T.D. Waite, K. Hanna, Environ. Sci. Technol. 52 (2018) 12010–12025.
[5] A. Liu, J. Liu, W.X. Zhang, Chemosphere 119 (2015) 1068–1074.
[6] Z. Xiong, B. Lai, P. Yang, Chemosphere 194 (2018) 189–199.
[7] M. Gheju, Water Air Soil Pollut. 222 (2011) 103–148.
[8] Y.H. Huang, T.C. Zhang, Water Res. 39 (2005) 1751–1760.
[9] K. Ritter, M.S. Odziemkowski, R.W. Gillham, J. Contam. Hydrol. 55 (2002) 87–111.
[10] Y. Sun, J. Li, T. Huang, X. Guan, Water Res. 100 (2016) 277–295.
[11] X. Guo, Z. Yang, H. Dong, et al., Water Res. 88 (2016) 671–680.
[12] H. Qin, J. Li, H. Yang, et al., Environ. Sci. Technol. 51 (2017) 5090–5097.
[13] T. Liu, X. Li, T.D. Waite, Environ. Sci. Technol. 47 (2013) 7350–7356.
[14] D. He, J. Ma, R.N. Collins, T.D. Waite, Environ. Sci. Technol. 50 (2016) 3820–3828.
[15] Y. Mu, F. Jia, Z. Ai, L. Zhang, Environ. Sci. Nano 4 (2017) 27–45.
[16] Z. Xiong, B. Lai, Y. Yuan, et al., Chem. Eng. J. 302 (2016) 137–145.
[17] H. Zhang, Q. Ji, L. Lai, G. Yao, B. Lai, Chin. Chem. Lett. 30 (2019) 1129–1132.
[18] M. Zhu, L. Zhang, S. Liu, et al., Chin. Chem. Lett. 31 (2020) 1961–1965.
[19] M.S. Odziemkowski, R.P. Simpraga, Can. J. Chem. 82 (2004) 1495–1506.
[20] X. Guan, Y. Sun, H. Qin, et al., Water Res. 75 (2015) 224–248.
[21] L. Liang, X. Guan, Z. Shi, et al., Environ. Sci. Technol. 48 (2014) 6326–6334.
[22] V. Sarathy, P.G. Tratnyek, J.T. Nurmi, et al., J. Phys. Chem. C 112 (2008) 2286–2293.
[23] H. Xu, Y. Sun, J. Li, F. Li, X. Guan, Environ. Sci. Technol. 50 (2016) 8214–8222.
[24] L. Santos-Juanes, F.S. García Einschlag, A.M. Amat, A. Arques, Chem. Eng. J. 310 (2017) 484–490.
[25] J. Yu, X. Hou, X. Hu, et al., Appl. Catal. B 256 (2019)117876.
[26] H. Qin, Y. Sun, H. Yang, et al., Chem. Eng. J. 334 (2018) 296–304.
[27] Y. Sun, X. Guan, J. Wang, et al., Environ. Sci. Technol. 48 (2014) 6850–6858.

[28] Y. Ren, J. Li, L. Lai, B. Lai, Chemosphere 194 (2018) 634–643.
[29] B. Lai, Y. Zhang, Z. Chen, et al., Appl. Catal. B 144 (2014) 816–830.
[30] H. Dong, F. Zhao, G. Zeng, et al., J. Hazard. Mater. 312 (2016) 234–242.
[31] A. Liu, J. Liu, J. Han, W.X. Zhang, J. Hazard. Mater. 322 (2017) 129–135.
[32] D. O'Carroll, B. Sleep, M. Krol, H. Boparai, C. Kocur, Adv. Water Resour. 51 (2013) 104–122.
[33] D.D. Boland, R.N. Collins, C.J. Miller, C.J. Glover, T.D. Waite, Environ. Sci. Technol. 48 (2014) 5477–5485.
[34] Y. Yang, Y. Zhang, J.C. Shen, et al., Chin. Chem. Lett. 27 (2016) 891–895.
[35] L. Chekli, B. Bayatsarmadi, R. Sekine, et al., Ana. Chim. Acta 903 (2016) 13–35.
[36] H. Xu, Y. Sun, J. Li, F. Li, X. Guan, Environ. Sci. Technol. 50 (2016) 8214–8222.
[37] J. Li, Y. Wan, Y. Li, G. Yao, B. Lai, Appl. Catal. B 256 (2019) 117782.
[38] P.C.J. Graat, M.A.J. Somers, Appl. Surf. Sci. 100–101 (1996) 36–40.
[39] T. Yamashita, P. Hayes, Appl. Surf. Sci. 254 (2008) 2441–2449.
[40] J.E. Martin, A.A. Herzing, W. Yan, et al., Langmuir 24 (2008) 4329–4334.
[41] B. Shen, C. Dong, J. Ji, M. Xing, J. Zhang, Chin. Chem. Lett. 30 (2019) 2205–2210.
[42] D.Q. Yang, E. Sacher, J. Phys. Chem. C (2009) 6418–6425.
[43] J. Yan, J. Peng, L. Lai, et al., Environ. Sci. Technol. 52 (2018) 14302–14310.
[44] C. Tan, N. Gao, Y. Deng, et al., J. Hazard. Mater. 276 (2014) 452–460.
[45] X. Hu, B. Liu, Y. Deng, et al., Appl. Catal. B 107 (2011) 274–283.
[46] L. Xu, J. Wang, Environ. Sci. Technol. 46 (2012) 10145–10153.
[47] M.J. Alowitz, M.M. Scherer, Environ. Sci. Technol. 36 (2002) 299–306.
[48] Y. Mu, Z. Ai, L. Zhang, Environ. Sci. Technol. 51 (2017) 8101–8109.
[49] J. Li, Y. Li, Z. Xiong, G. Yao, B. Lai, Chin. Chem. Lett. 30 (2019) 2139–2146.
[50] A. Fischbacher, J. von Sonntag, C. von Sonntag, T.C. Schmidt, Environ. Sci. Technol. 47 (2013) 9959–9964.
[51] M. Tong, S. Yuan, S. Ma, et al., Environ. Sci. Technol. 50 (2016) 214–221.